THEORETICAL AND EXPERIMENTAL INVESTIGATION OF A DOUBLE-LAP ADHESIVE JOINT WITH GLASS FIBER REINFORCED POLYMER TO PLYWOOD INTERFACE

Catherine Lester, Malo Rosemeier, Moritz Bätge, and Alexandros Antoniou

Division Structural Components, Fraunhofer IWES, Fraunhofer Institute for Wind Energy Systems,
Am Seedeich 45, 27572 Bremerhaven, Germany
Email: catherine.lester@iwes.fraunhofer.de, Web Page: http://www.iwes.fraunhofer.de

Keywords: sub-component testing, adhesive lap joint, experimental validation, digital image correlation

Abstract
Wind turbine rotor blade full-scale tests utilize plywood load frames to introduce forces normal to the length of the blade. Plywood frames are low cost and easily milled to the unique profile of a rotor blade. A sub-component test supplements full-scale tests by focusing on a region exposed to specific loading scenarios. However, these tests require an upgraded load introduction frame capable of introducing axial forces and bending moments. To develop such a frame structure, a generic small-scale load introduction frame was designed and proved as a concept in this work. The specimen was a double-lap shear adhesive joint bonding a glass fiber reinforced polymer composite, representing the blade, to plywood, representing the frame, tested under uni-axial tension. The bond line of the specimen was modeled analytically and numerically. A digital image correlation system recorded the experimental full-field strain. Furthermore, a validation of the models was performed.

1. Introduction

Wind turbine rotor blade full-scale testing (FST) is used for the certification of a new blade type. However, interest in a small region of the blade does not necessitate FST. In particular, fatigue testing in resonance has downsides including limited load combinations and high local overloading [1]. Furthermore, local failures require the investigation of potential design modifications or alternative solutions, which require multiple, relatively quick tests [2].

Recently, sub-component testing (SCT) was proposed as a complement to the full-scale test [2-5]. With SCT, a blade segment is cut or manufactured separately. While in FST the load is introduced transverse to the blade span (Figure 1a), in SCT the load is introduced axially into the specimen via plywood load frames which are glued to the blade's glass fiber reinforced polymer (GFRP) structure (Figure 1b). The axial loads are thus transferred via a shear-loaded adhesive layer.

The materials of the joint system, substrate – adhesive – substrate, play a substantial role in the structural performance. A higher adhesive strength does not always yield a stronger joint. Higher adherend stiffness results in higher adhesive stresses, i.e. von Mises and peel [6], and can lead to composite failure [7]. Kahn et al. studied the effect of a more ductile adhesive in a single lap joint. They found cohesive failure dominates low modulus adhesives, while stiffer adhesives fail at the interface [8].

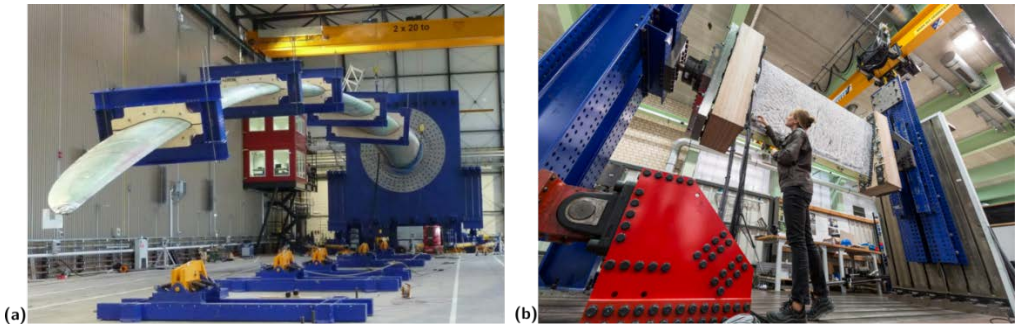

Figure 1. Load frames used in a full-scale rotor blade test (a) and in a sub-component test (b) [13].

Volkersen [9] was the first to analyze bonded joints with a model of the adhesive shear stress distribution in a single lap joint. Since the model was created for a single lap joint, it did not include the eccentric load in the asymmetric joint, resulting in a bending moment and a transverse force. Goland and Reissner [10] and Hart-Smith [11] accounted for the rotation in the asymmetric joint. Tsai et al. [12] advanced Volkersen's model to include adherend shear and different material properties of the inner and outer-adherends.

This work presents a generic specimen which represents the load introduction joint capable of introducing axial loads for SCT of rotor blades. The plywood load frame glued to a wind turbine rotor blade segment was scaled down and simplified to a double-lap joint specimen. The specimen consisted of a GFRP bonded to plywood because the load-carrying structure of a rotor blade is commonly made of GFRP. Several adherend configurations were investigated experimentally with a focus on optimizing the static strength of the joint. Additionally, analytical and numerical design models were validated with experimental results.

2. Methodology

2.1. Specimen and experiment design

The axial load-introducing frame (Figure 1b) was simplified to double-lap adhesive joints (Figure 2). In this experiment, the inner adherend was a GFRP plate. The outer adherend remained plywood due to the benefits it provides in respect of cost efficiency and low weight. Epoxy bonding paste was used as the adhesive.

The dimensions of the specimen are given in Table 1. The GFRP was designed to be very thin, to compensate for misalignments in the specimen or off-axis loading. Each plywood block was bolted above and below to steel plates to generate pure shear without any peeling or bending. The setup configuration was designed to have pure shear, which is idealistic, but representative of the application.

Table 1. Specimen dimensions as labeled in Figure 2.

Component	Dimension	Label	Value in mm
GFRP adherend	Thickness	t_g	4.5
GFRP adherend	Height	h_g	500.0
Plywood adherend	Height	h_p	60.0
Adhesive	Thickness	t_a	5.0
Steel plates	Thickness	t_s	15.0

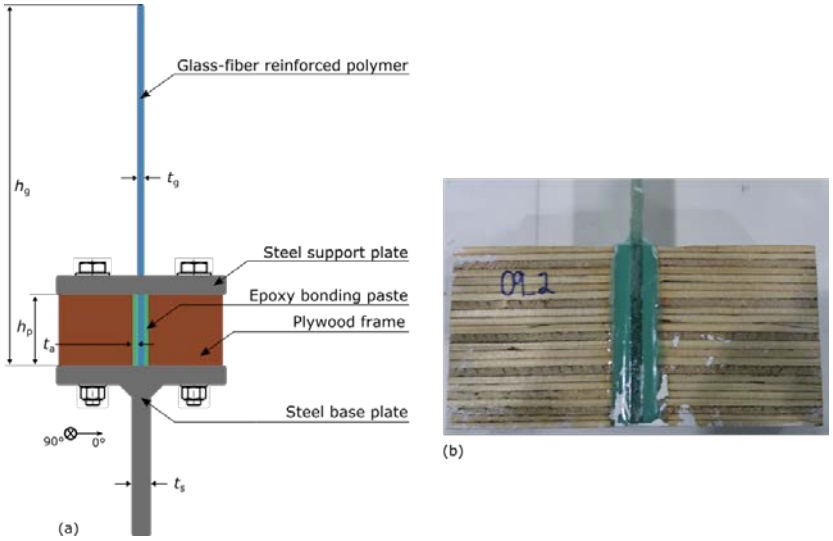

Figure 2. Principle drawing of specimen design with labeled dimensions (a) and actual specimen (b).

This experiment aimed to predict the behavior of double-lap joints. Furthermore, the design allowable, i.e., the maximum load that the joint can carry, was determined. In SCT, the object of interest is the blade section. Static tensile loads were applied until failure in a calibrated 250kN universal servo-hydraulic coupon machine with a controlled displacement of 0.5mm/min.

The plywood orientation and the adhesive system were the variables of interest. Three birch plywood stacking sequences were investigated: (0_{22}), $((90/0)_7/90)_3$ and $(0_2/90/0_4/90/0_3/\overline{90})_s$ (Figure 2b). In an additional specimen the interface material was changed by wrapping a thin steel plate around a plywood block. Three adhesives of varying stiffnesses and strengths were used (Table 2).

Table 2. Adhesive materials used.

Adhesive	Elastic modulus in MPa	Shear modulus in MPa
High modulus	5500	2040
Medium modulus	500	185
Low modulus	3	1

2.2. Analytical models

Tsai's model was used because it considers the inner and the outer adherends as different materials. The adhesive shear stress distribution along the bond line is defined as

$$\tau_o = A \sinh(\beta x) + B \cosh(\beta x) \quad (1)$$

The coefficients A and B are defined as

$$A = \frac{\beta c \tau_{avg}}{cosh(\beta c)} \cdot \left[\frac{1 - \frac{E_i t_i}{2 E_o t_o}}{1 + \frac{E_i t_i}{2 E_o t_o}} \right] \qquad B = \frac{\beta c \tau_{avg}}{sinh(\beta c)} \quad (2)$$

where the inner adherend (GFRP) properties are used: longitudinal elastic modulus, shear modulus and thickness, represented by E_i, G_i and t_i, respectively. The plywood is the outer adherend, which is represented by E_o, G_o and t_o. Finally, the adhesive shear modulus and thickness are G_a and t_a.

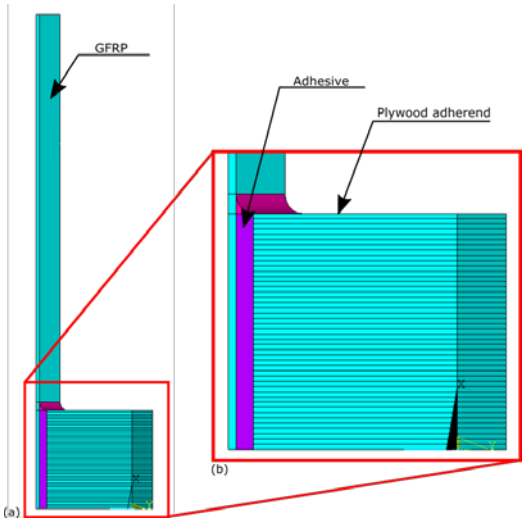

Figure 3. Finite element model of symmetrical quarter specimen (a) and zoom of adhesive and adherend region. The adhesive is modeled as two element types and one material definition (b).

The coefficient β is defined as

$$\beta = \frac{\frac{G_a}{t_a}\left(\frac{2}{E_i t_i} + \frac{1}{E_o t_o}\right)}{1 + \frac{G_a}{t_a}\left(\frac{t_i}{6G_i} + \frac{t_o}{3G_o}\right)} \tag{3}$$

2.3. Finite element model

A finite element model of a double-lap joint was implemented in ANSYS APDL [14]. The model exactly reproduced the geometry of a double-lap joint [15]. Two axes of symmetry allowed one quarter of the specimen to be modeled (Figure 3a). Boundary conditions fixed the top and bottom surface of the plywood in all degrees of freedom. In the experiment, thick steel plates held the plywood in place. It was assumed the plates were sufficiently stiff to prevent bending and peeling. A mesh size convergence study was performed.

The adhesive and adherends were modeled as solid elements [16]. The adhesive was modeled in two parts, seen in Figure 3b. The purple rectangular region in contact with the plywood and the GFRP was modeled as a SOLID186. The pink tapered region of the adhesive was modeled as a SOLID187. The GFRP was modeled with SHELL181 and the plywood with SOLID186.

2.4. Digital image correlation

The experiment was recorded using Digital Image Correlation (DIC), a noncontact, full-field deformation measurement system. A series of images are compared with a reference image captured at zero load and zero strain [17], seen in this experiment in Figure 4a. A stochastic black and white speckle pattern painted on the specimen surface is divided into subset blocks [17] and analyzed by means of an advanced pixel recognition and interpolation algorithm [18]. Two 2.8 megapixel cameras recorded three-dimensional movements at 1.5Hz. Istra4D software calculated a surface strain map.

It was assumed that the adhesive exhibits linear-elastic behavior at the low load; thus the shear strain values were multiplied by the manufacturer's shear modulus to obtain the shear stress:

$$\tau = G\varepsilon \tag{4}$$

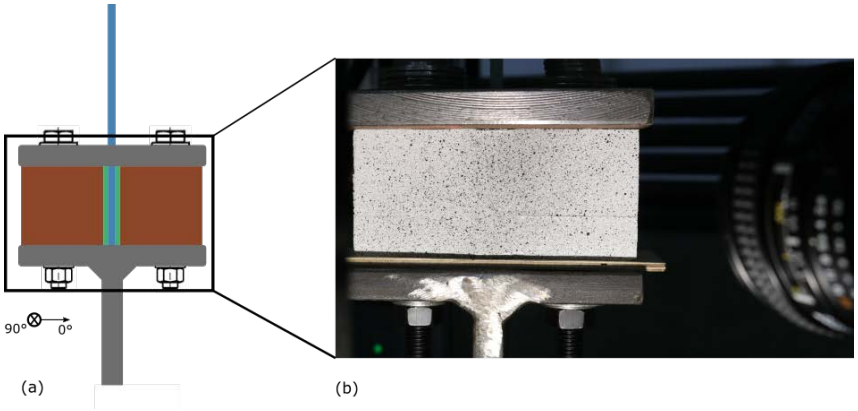

Figure 4. DIC requires two cameras focused on the area of interest, seen boxed in the principle drawing (a) and the actual painted specimen in the test machine (b). The coordinates indicate the plywood orientation.

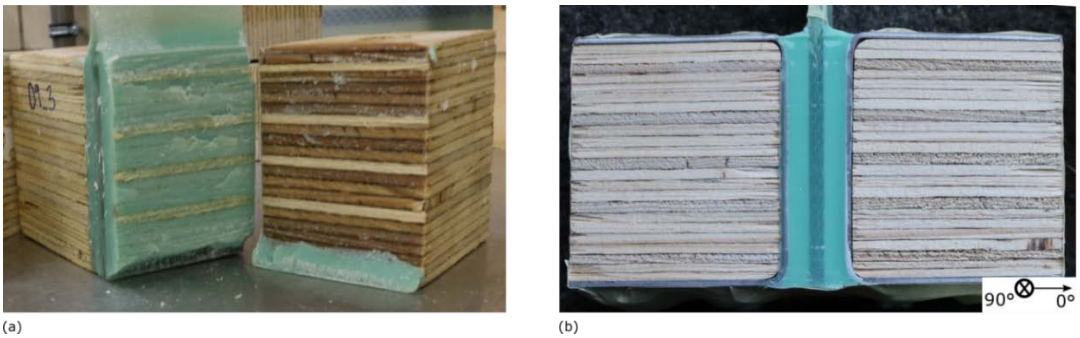

Figure 5. Experimental specimens: failed plywood adherend (a). Some fibers from the 90° plies remain attached, whereas the 0° plies have left little residue. The steel wrapped plywood specimen before testing (b).

3. Results and discussion

3.1. Experimental failure results

The test matrix of this experiment included three plywood materials and one steel sheet wrapped around a plywood block. At failure, the 0° plies left minimal residue on the adhesive surface (the tips of the fiber were in contact with the adhesive). The 90° wood fibers, however, remained on the adhesive surface. The steel-wrapped block provided an alternative interface for the adhesive (Figure 5b). This configuration did not add significant mass to the specimen, although it doubled the shear strength compared to the best laminate-to-plywood configuration (Figure 6).

Further investigations included a test series of three adhesives, all with (0_{22}) plywood. The stiffest adhesive could withstand 33% higher shear stress than the others. The most ductile adhesive experienced cohesive failure and the others failed at the interface, in agreement with [8].

In the 90° plies, the wood fibers were ripped away from neighboring fibers (Figure 5a). Higher shear strain in these plies is visible in the DIC shear strain map in Figure 7b.

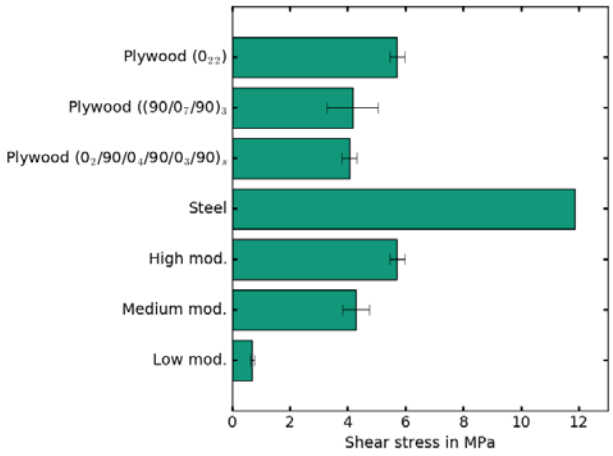

Figure 6. Experim. results of the shear stress at failure, defined as max. load divided by the bond area.

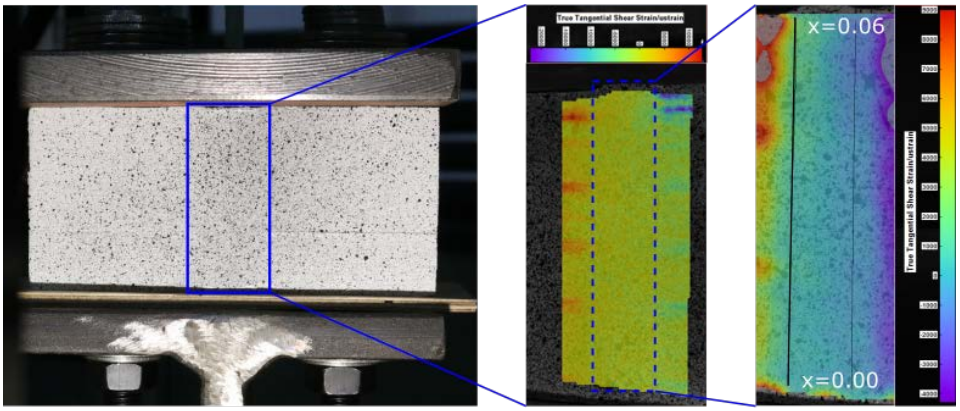

Figure 7. DIC results: painted specimen with area of interest in blue box (a), shear strain field map overlaid on specimen (b). The dashed box surrounds the adhesive and GFRP. The 0° plies shear strain max. seen as red and blue/green in the color map. The shear strain field map of the adhesive and GFRP (c). The shear strain distribution line, equivalent to the analytical model, marked by a black line.

3.2. Validation results

In the model validation, the test series analyzed was of plywood $((90/0)_7/90)_3$ and the stiffest adhesive. The shear stress distribution at 15kN is shown in Figure 8. The models are in agreement with experimental results, except at the peak stress.

DIC was used to record the shear strains along the bond line of the surface, as shown in Figure 8b. The equivalent shear strain distribution was measured along a line at the outermost side of the bond line, seen as the black line from x=0 to x=0.06 in Figure 8b. The corresponding stresses were calculated as described in section 1.4 and are plotted in Figure 8a.

The fluctuant shape of the experimental (and less so the numerical) curve is likely due to the alternating ply orientation of plywood. Thin adhesives yielded DIC results with a high degree of scatter, which could be compensated by attaching an optical lens to the DIC cameras [18].

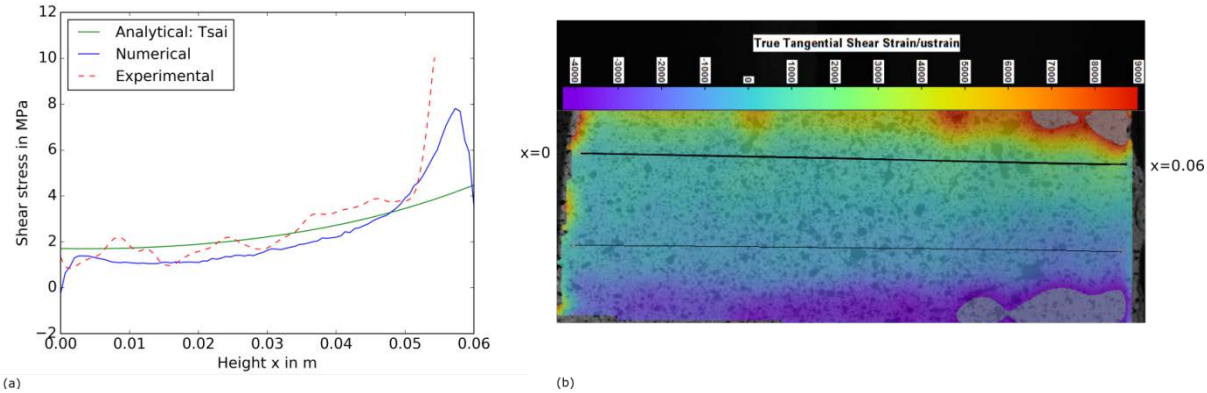

Figure 8. Shear stress distribution along bond line of test specimen with high stiffness and plywood $((90/0)_7/90)_3$; analytical, numerical and experimentally derived stresses (a). Strain map DIC (b).

4. Conclusions

The traditional load frame used in full-scale rotor blade tests must be redesigned for use in a sub-component test, which requires axial loads to mimic the loads of wind turbines in the field. Based on the generic sub-component load frame, a double-lap adhesive joint was designed and tested with the purpose of deriving experimental, design-permissible strength values.

The adherend was varied between three plywood orientations and a steel plate. The latter outperformed all plywood interfaces. The failure occurred at the outer adherend – adhesive interface. The high modulus adhesive outperformed the others. The failure modes of the joints were in agreement with the literature: very stiff bond lines fail at the interface, and elastic adhesives have cohesive failure.

The Tsai analytical model and the finite element model fit well with the experimental data recorded by the two-camera DIC system. The good agreement between the DIC and the analytical/numerical results is an indirect indication that the shear strain distribution of the bond line was measured successfully with a given accuracy.

The analytical model predicted the stress peak with a difference of at least 100% from the derived numerical model and experimental results. A safety factor larger than 2 would be required if the Tsai model was to be used for design purposes.

Acknowledgments

The authors acknowledge the support provided by the German Federal Ministry for Economic Affairs and Energy (BMWi) (0325939) as a part of the Future Concept Fatigue Strength of Rotor Blades project and by the Senator for Health, Environment and Consumer Protection of the Free Hanseatic City of Bremen within the ERDF program Bremen 2014-2020 (201/PF_IWES_Zukunftskonzept_ Betriebsfestigkeit_Rotorblaetter_Phase_I).

References

[1] M. Rosemeier, M. Bätge and A. Antoniou. A novel single actuator test setup for combined loading of wind turbine rotor blade sub-components. *Proceedings of the 2nd International Symposium on Multiscale Experimental Mechanics: Multiscale Fatigue in Lyngby, Denmark,* 2017.

[2] A. van Wingerde, F. Sayer, A. Antoniou, F. Bürkner and E. Putnam. Subcomponent testing for rotor blades of wind turbines. *The 19th International Conference on Composite Materials*, Paris, 2017.

[3] K. Branner, P. Berring and P. U. Haselbach. Subcomponent testing of trailing edge panels in wind turbine blades. *Proceedings of 17th European Conference on Composite Materials*, 2016.

[4] F. Lahuerta, M. J. d. Ruiter, L. Espinosa, N. Koorn and D. Smissaert. Assessment of wind turbine blade trailing edge failure with sub-component tests. *Proceedings of 21st International Conference on Composite Materials ICCM21*, Xi'an, 2017.

[5] M. Rosemeier, G. Basters and A. Antoniou. Benefits of subcomponent over full-scale blade testing elaborated on a trailing-edge bond line design validation. *Wind Energy Science*, vol. 3 (1), pp. 163-172, 2018.

[6] M. Mokhtari, K. Madani, M. Belhouari, S. Touzain, X. Feaugas and M. Ratwani. Effects of composite adherend properties on stresses in double lap bonded joints. *Materials and Design*, vol. 44, pp. 633-639, 2013.

[7] M. D. Banea and L. F. M. da Silva. Adhesively bonded joints in composite materials: an overview. *The Journal of Materials: Design and Applications*, vol. 223, no. 1, pp. 1-18, 2009.

[8] M. Kahn, G. Aglietti, A. Crocombe, A. Viquerat and C. Hamar. Development of design allowables for the design of composite bonded double-lap joints in aerospace applications. *International Journal of Adhesion and Adhesives*, vol. 82, pp. 221-232, 2018.

[9] O. Volkersen. Nietktraftverteilung in zugbeanspruchten Nietverbindungen mit konstanten Laschenquerschritten. *Luftfahrtforschung*, vol. 15, pp. 41-47, 1938.

[10] M. Goland and E. Reissner. Stresses in cemented joints. *J. appl. Mech*, vol. 66, pp. A17-A27, 1944.

[11] L. Hart-Smith, Adhesive-bonded double-lap joints, NASA Contract Report, 1973.

[12] M. Tsai and J. Morton. An investigation into the stresses in double-lap adhesive joints with laminated composite adherends. *International Journal of Solids and Structures*, vol. 47, pp. 3317-3325, 2010.

[13] M. Rosemeier, A. Antoniou and C. Lester. Sub-Components of Wind Turbine Blades - Proof of a Novel Trailing Edge Testing Concept. *Conference Proceedings of the Society for Experimental Mechanics Series*, 2018.

[14] J. Swanson. ANSYS Mechanical APDL. Version 15.0, 2013.

[15] A. Spaggiari. Efficient modelling of complex adhesively bonded structures by standard finite element techniques. University of Modena e Reggio Emilia, 2009.

[16] E. Armentani, M. Laiso, F. Caputo and R. Sepe. Numerical FEM Evaluation for the Structural Behaviour of a Hybrid (bonded/bolted) Single-lap Composite Joint. *International Conference on Stress Analysis AIAS 2017* , Pisa, Italy, 2017.

[17] A. Comer, K. Katnam, W. Stanley and T. Young. Characterising the behaviour of composite single lap bonded joints using digital image correlation. *International Journal of Adhesion & Adhesives*, vol. 40, pp. 215-223, 2013.

[18] K. Colavito, J. Gorman and E. Madenci. Refinements in Digital Image Correlation Technique to Extract Adhesive Strains in Lap joints. *AIAA/ASME/ASCE/AHS/ASC Structures, Structural Dynamics and Materials Conference*, Palm Springs, California, 2009.

[19] ASTM D3528. Strength properties testing of double lap shear adhesive joints by tension loading, 2016.

[20] L. da Silva, P. das Neves, R. Adams and J. Spelt. Analytical models of adhesively bonded joints-Part I: Literature survey. *International Journal of Adhesion and Adhesives*, vol. 29, pp. 319-330, 2009.